Analytical Modeling for Stress-Strain Curve of a Porous NiTi

Ying Zhao

Minoru Taya
e-mail: tayam@u.washington.edu

Department of Mechanical Engineering,
University of Washington,
Box 352600,
Seattle, WA 98195-2600

Two models for predicting the stress-strain curve of porous NiTi under compressive loading are presented in this paper. Porous NiTi shape memory alloy is considered as a composite composed of solid NiTi as matrix and pores as inclusions. Eshelby's equivalent inclusion method and Mori-Tanaka's mean-field theory are employed in both models. Two types of pore connectivity are investigated. One is closed cells (model 1); the other is where the pores are interconnected to each other forming an open-cell microstructure (model 2). We also consider two different shapes of pores, spherical and ellipsoidal. The stress-strain curves of porous shape memory alloy with spherical pores and ellipsoidal pores are compared. It is found that the ellipsoidal shape assumption is more reasonable than the assumption of spherical pores. Comparison of the stress-strain curves of the two models shows that use of open-cell microstructure (model-2) makes the predictions more agreeable to the experimental results of porous NiTi whose microstructure exhibits open-cell microstructure. [DOI: 10.1115/1.2198250]

1 Introduction

Over the last two decades shape memory alloys (SMAs) have attracted great interests in various applications ranging from aerospace [1] and naval structures [2] to surgical instruments, medical implants and fixtures [3,4]. The use of SMAs has promoted extensive researches on developing SMA constitutive models.

Among SMAs, NiTi alloy has been used most extensively due to its large flow stress and shape memory effect (SME). Most recently, porous NiTi attracted an increasing attention as a possible application to medical implant devices and high energy absorption structural material and potential material for surface cooling. The progress in both manufacturing and characterization of the porous NiTi SMA has been reported by a number of researchers. A short review of the existed processing methods is presented here. Li et al. [5,6] fabricated porous NiTi SMA by combustion synthesis method, the stress-strain curves in their work exhibit brittle behavior. Li et al. [7] also fabricated the porous NiTi by powder sintering; it shows that the there is no stress plateau in the stress-strain curve and the material is still brittle. Some studies [8,9] report superelastic behavior of the foams in compression, but stresses are low due to the high porosity. Lagoudas et al. [10] used the HIP (hot isostatic press) method and the stress-strain curve in their work showing brittle behavior. Recently, we processed the porous NiTi by the spark plasma sintering (SPS) method, and the specimens exhibit large superelastic loop with high stress flow and high ductility [11].

In order to make an optimum design of the microstructure of the porous SMAs, it is important to construct a simple, yet accurate model to describe its microstructure-mechanical behavior relation. Thus far, there are few analytical studies focused on the porous SMA, particularly no analytical model for the porous SMA with open porosity. Therefore, in this paper two models are introduced. The porous NiTi is treated as a composite with solid NiTi as its matrix and pores as the inclusions. If a porous NiTi can be viewed as a special or ellipsoidal inclusion case of a particular reinforced composite, then one can construct a micromechanical model based on Eshelby's equivalent inclusion method [12] with Mori-Tanaka mean-field theory [13]. In the first model (model 1), the pores in the porous NiTi are closed, i.e., pores are not connected to each other. In the second model (model 2), pores are assumed to be connected to each other, i.e., open porosity microstructure. Effects of pores with different geometries (spherical and ellipsoidal) are also studied in both models.

There are two advantages of these models. First, it is a simpler model. We need less input data, and the input data for our model are taken from the experimental stress-strain curve of the solid NiTi, i.e., no need to manipulate types of matensite variants, their orientations, etc., often used by other models. Second, in the literature, there exists no model that treated porous NiTi with the open-cell structure. The model proposed in this paper is the first in treating the open-cell structure within the framework of Eshelby's model.

In the following, we shall state first two constitutive models, model 1 (Sec. 2) and model 2 (Sec. 3) and discuss the resulting stress-strain curves they predict. This response will be compared to previous experimental results, [11], and conclusions will be presented.

2 Model-1: Stress-Strain Curve of Porous NiTi With Closed Pores

The stress-strain curve of a SMA with superelastic grade is assumed to be composed of four stages; see Fig. 1. The first stage (I) is a linear elastic stage, with the matrix of 100% austenite. The second stage (II) is a stress-induced matensitic transformation stage; in this stage, a volume fraction of the austenite decreases from 100% to 0% while that of the martensite increases from 0% to 100%, continuously. The third stage (III) is a stage with the matrix of 100% matensite. Therefore, the third stage is an linear elastic stage. The fourth stage (VI) is the austenite transformation stage, in which the volume fraction of martensite changes from 100% to 0% while that of the austenite in the matrix increases from 0% to 100%. $\sigma^P_{M_s}$, $\sigma^P_{M_f}$, $\sigma^P_{A_s}$, and $\sigma^P_{A_f}$ are the critical stresses between the above four stages, the superscript P denotes porous and subscripts M_s, M_f, A_s, and A_f denote martensite start, martensite finish, austenite start, and austenite finish, respectively. E_{M_s} and E_{M_f} are the moduli of the first and third stages and E_T is the

Contributed by the Applied Mechanics Division of ASME for publication in the JOURNAL OF APPLIED MECHANICS. Manuscript received April 7, 2005; final manuscript received January 17, 2006. Review conducted by M. R. Begley. Discussion on the paper should be addressed to the Editor, Prof. Robert M. McMeeking, Journal of Applied Mechanics, Department of Mechanical and Environmental Engineering, University of California-Santa Barbara, Santa Barbara, CA 93106-5070, and will be accepted until four months after final publication of the paper itself in the ASME JOURNAL OF APPLIED MECHANICS.

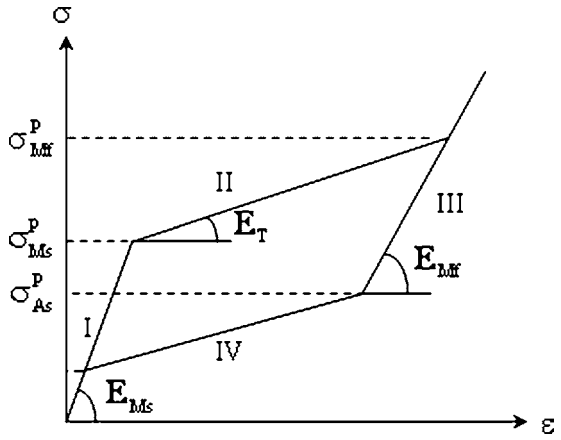

Fig. 1 Linearized four-stage stress-strain curve of porous NiTi

tangent modulus of the second and fourth stages. It is noted that the slope of the forth stage is the same as that of the second stage. In this paper, we use the stress-strain curve of the solid NiTi (i.e., without pores) as a reference.

2.1 Eshelby Model for a Porous SMA With Closed Pores. Consider an Eshelby model for a porous NiTi with closed pores subjected to applied stress σ^0_{ij} where the matrix is solid with uniform martensite transformation strain ε^T_{ij} (Fig. 2(*a*)). The uniform transformation strain ε^T_{ij} is assumed only for the second and fourth stages, while for the first and third stages, $\varepsilon^T_{ij}=0$. In the Eshebly's model, an infinite elastic body (D), which contains spherical or ellipsoidal pores (Ω_p), is subjected to a uniform stress σ^0_{33} as shown in Fig. 2. As far as the stress field is concerned, the model of Fig. 2(*a*) is equivalent to that of Fig. 2(*b*) where the uniform transformation strain in the matrix is removed from and added with minus sign to the pore domain. Thus, the present problem is reduced to the inhomogeneous inclusion problem where the elastic stiffness tensor C^m_{ijkl} is homogeneous in the entire domain D, Fig. 2(*b*) [14].

The Eshelby's inhomogeneous inclusion problem with Mori-Tanaka's mean field theory provides the total stress field given by

$$\sigma^0_{ij}+\sigma_{ij}=\mathbf{C}^m_{ijkl}[e^0_{kl}+\bar{\varepsilon}_{kl}+\varepsilon_{kl}-(\varepsilon^*_{kl}-\varepsilon^T_{kl})]$$
$$=\mathbf{C}^m_{ijkl}(\varepsilon^0_{kl}+\bar{\varepsilon}_{kl}+\varepsilon_{kl}-\varepsilon^{**}_{kl})=\mathbf{C}^p_{ijkl}(\varepsilon^0_{kl}+\bar{\varepsilon}_{kl}+\varepsilon_{kl}) \quad (1)$$

where $\mathbf{C}^m_{ijkl}$ and $\mathbf{C}^P_{ijkl}$ are the elastic stiffness tensor of matrix and pores, respectively. σ_{ij} and ε_{kl} are stress and strain disturbance due to existence of pores, respectively. $\bar{\varepsilon}_{kl}$ is the average strain disturbance in the matrix due to the pores (Ω_p). ε^*_{ij} is the fictitious eigenstrain, which has nonvanishing components in the domain Ω_p. Here, we introduce

$$\varepsilon^{**}_{kl}\equiv\varepsilon^*_{kl}-\varepsilon^T_{kl} \quad (2)$$

For the entire domain D, the following relation always holds:

$$\sigma^0_{ij}=\mathbf{C}^m_{ijkl}\varepsilon^0_{kl} \quad (3)$$

Following the Mori-Tanaka mean filed theory, the average stress disturbance in the matrix, $\langle\sigma_{ij}\rangle_m$ is given by

$$\langle\sigma_{ij}\rangle_m=\mathbf{C}^m_{ijkl}\bar{\varepsilon}_{kl} \quad (4)$$

The strain disturbance is related to ε^{**}_{mn} as

$$\varepsilon_{kl}=\mathbf{S}_{klmn}\varepsilon^{**}_{mn} \quad (5)$$

The requirement that integration of the stress disturbance over the entire body (D) vanishes, leading to

$$\bar{\varepsilon}_{kl}=-f_P(\mathbf{S}_{klmn}\varepsilon^{**}_{mn}-\varepsilon^{**}_{kl}) \quad (6)$$

where $\mathbf{S}_{klmn}$ is Eshelby's tensor for pore inclusion and its exact values are given in Appendix and f_p is the volume fraction of pore, i.e., porosity of the SMA. A substitution of Eq. (3)–(6) into (1) provides a solution for ε^{**}_{kl}

$$\varepsilon^{**}_{ij}=\{(1-f_P)\mathbf{C}^m_{ijkl}(\mathbf{S}_{klmn}-\mathbf{I}_{klmn})+\mathbf{C}^P_{ijkl}[(1-f_P)\mathbf{S}_{klmn}+f_P]\}^{-1}(\mathbf{C}^P_{mnst}\mathbf{C}^{m-1}_{stpq}-\mathbf{I}_{mnpq})\sigma^0_{pq} \quad (7)$$

where $\mathbf{I}$ is identity matrix of 6×6. In this paper boldface symbols ($\mathbf{S},\mathbf{C},\mathbf{I}$), are fourth-order tensor, and they are converted to 6×6 matrix form for facilitation of calculation. These boldface symbols with subscripts should be written as not boldface with subscript when they are scalar components. However, to avoid confusion, we keep boldface symbols.

As the stiffness of the pores is zero, $\mathbf{C}^P_{ijkl}=0$; thus, Eq. (7) is given as

$$\varepsilon^{**}_{mn}=-\frac{1}{1-f_P}(\mathbf{S}_{klmn}-\mathbf{I}_{klmn})^{-1}C^{m-1}_{ijkl}\sigma^0_{ij} \quad (8)$$

By setting $\mathbf{C}^P_{ijkl}=0$, Eq. (1) becomes

$$\sigma^0_{ij}=-\sigma_{ij} \quad (9)$$

Next, we shall consider the strain energy density of the inhomogeneous inclusion problem of Fig. 2(*b*), which is given by [15]

$$W_{mi}=\frac{1}{2}\sigma^0_{ij}\varepsilon^0_{ij}+\frac{1}{2}f_P\sigma^0_{ij}\varepsilon^*_{ij}-\frac{1}{2}f_P\sigma_{ij}\varepsilon^T_{ij} \quad (10)$$

Let us call W_{mi} as microscopic strain energy density. It is noted in Eq. (10) that W_{mi} is valid for all three stages, i.e., for the first and third stages $\varepsilon^T_{ij}=0$, whereas for the second stage, all three terms on the right-hand side of Eq. (10) are nonvanishing.

2.1.1 Stiffness of First and Third Stages. The equivalency of strain energy density of porous SMA for the first and third stages can be derived from Eq. (10) with $\varepsilon^T_{ij}=0$, which is set equal to the strain energy density of a porous SMA with its elastic stiffness tensor $\mathbf{C}^c_{ijkl}$, where c refers to "composite," as porosity is a special case of composite.

$$\frac{1}{2}\mathbf{C}^{c-1}_{ijkl}\sigma^0_{ij}\sigma^0_{kl}=\frac{1}{2}\mathbf{C}^{m-1}_{ijkl}\sigma^0_{ij}\sigma^0_{kl}+\frac{1}{2}f_P\sigma^0_{ij}\varepsilon^*_{ij} \quad (11)$$

where $\mathbf{C}^{c-1}_{ijkl}$ and $\mathbf{C}^{m-1}_{ijkl}$ are the elastic compliances of the composite and the matrix material (solid NiTi), respectively. Since only the nonvanishing component of σ^0_{ij} is $\sigma^0_{33}=\sigma_0$ (Fig. 2), Eq. (11) is reduced to

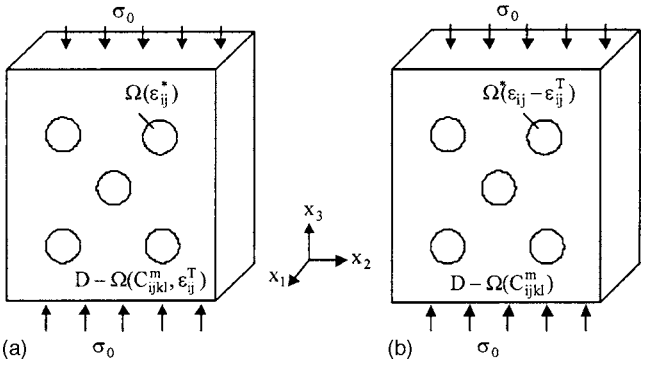

Fig. 2 The Eshelby's model for a porous SMA: (*a*) the problem of pores embedded in the NiTi matrix with stiffness C^m_{ijkl} and transformation strain ε^T_{ij}, which can be converted to equivalent inclusion problem (*b*), where ε^*_{ij} is the fictitious eigenstrain, which is unknown.

$$\frac{\sigma_0^2}{2E_c} = \frac{\sigma_0^2}{2E_m} + \frac{f_P}{2}\sigma_0\varepsilon_{33}^* \tag{12}$$

where E_c and E_m are the Young's moduli of the composite and the matrix, respectively. In the first stage, E_c is E_{M_s}, and E_m is the Young's modulus of austenite E_A. Combining Eq. (12) with Eq. (2) and (8) with $\varepsilon_{ij}^T=0$, the Young's modulus of the porous NiTi in the first stage, E_{M_s} normalized by E_A is given as

$$\frac{E_{M_s}}{E_A} = \frac{1}{1+\eta f_P} \tag{13}$$

where η is a parameter, a function of porosity f_P and shape of the porous inclusion

$$\eta = \frac{-(\mathbf{H}_{1133}+\mathbf{H}_{2233}+\mathbf{H}_{3333})}{(1-f_p)} \tag{14a}$$

$\mathbf{H}$ is a (6×6) matrix, which is given as

$$\mathbf{H}_{ijmn} = (\mathbf{S}_{ijkl}-\mathbf{I}_{ijkl})^{-1}\mathbf{C}_{klmn}^{-1} \tag{14b}$$

Young's modulus of the porous NiTi at the third stage, E_{M_f} can be obtained in the same manner as the above,

$$\frac{E_{M_f}}{E_M} = \frac{1}{1+\eta f_P} \tag{14c}$$

2.1.2 Critical Stresses $\sigma_{M_s}^P$ and $\sigma_{M_f}^P$. Under the uniaxial stress along the x_3-axis (σ_0), the transformation strain ε_{ij}^T is assumed to be uniform with the following components:

$$\varepsilon_{ij}^T = \{\nu\varepsilon^T \ \nu\varepsilon^T \ -\varepsilon^T \ 0 \ 0 \ 0\}^T \tag{15}$$

where ε^T is the transformation strain along x_3-axis.

The stress disturbance σ_{ij} is obtained from Eq. (9). The change of the total potential energy of the inhomogeneous inclusion of the problem of Fig. 2(*b*), δU, due to the change in transformation strain $\delta\varepsilon_{ij}^T$ is given by [16]

$$\delta U = -\delta\varepsilon_{ij}^T](1-f_P)\sigma_{ij}^0 - f_P\sigma_{ij}] \tag{16}$$

The work done by the applied stress δQ causing infinitesimal transformation strain $\delta\varepsilon_T$ is

$$\delta Q = (1-f_P)\sigma_{M_s}^S\delta\varepsilon_T \tag{17}$$

where $\sigma_{M_s}^S$ is the stress of the matrix at the onset of stress-induced martensite transformation, at the beginning of the second stage of the solid NiTi, the superscript S denotes solid material, and the subscript M_s denotes matensitic start transformation. Since $\delta U + \delta Q = 0$, we obtain

$$\sigma_0 = \sigma_{M_s}^S + \frac{f_P}{1-f_P}(\sigma_{33}-\sigma_{11}) \tag{18}$$

substituting $\sigma_{33}=-\sigma_0$ and $\sigma_{11}=0$ from Eq. (9) into Eq. (18), we obtain

$$\sigma_{M_s}^P = (1-f_P)\sigma_{M_s}^S \tag{19a}$$

The martensitic transformation finish critical stress $\sigma_{M_f}^P$ can be obtained in the same manner

$$\sigma_{M_f}^P = (1-f_P)\sigma_{M_f}^S \tag{19b}$$

2.1.3 Stiffness of Second Stage. Refer to Fig. 3(*a*), Young's modulus (E) of a SMA with transformation ε_T is estimated by

$$E(\varepsilon_T) = E_A + \frac{\varepsilon_T}{\varepsilon_{M_f}^T}(E_M - E_A) \tag{20}$$

where E_A, E_M are the Young's modulus of 100% austenite and 100% martensite phase, respectively, Fig. 3(*a*), and $\varepsilon_{M_f}^T$ is the maximum transformation strain, and it is given by

$$\varepsilon_{M_f}^T = \varepsilon_{M_f} - \frac{\sigma_{M_f}}{E_M} \tag{21}$$

Equation (20) is valid for both dense and porous SMA; thus, we can rewrite Eq. (20) using Eq. (21) as

$$E^i = E_A^i - \frac{E_A^i - E_M^i}{\varepsilon_{M_f}^i - \sigma_{M_f}^i/E_M^i}\varepsilon_T \tag{22}$$

where the superscript i denotes $i=S$ (solid) or P (porous). In order to obtain the slope of the linearized second stage of compressive stress-strain curve of a porous NiTi, we consider the equivalency of strain energy density. In addition, in the case of the second stage, we evaluate the macroscopic strain energy density of a porous NiTi graphically from Fig. 3(*a*), i.e., area enclosed by the curve. W_{ma} is given by

$$W_{ma} = \frac{1}{2}(\sigma_{M_s}^P + \sigma_0^P)\left(\varepsilon_T^P + \frac{\sigma_0^P}{E_{AM}} - \frac{\sigma_{M_s}^P}{E_{M_s}}\right) \tag{23}$$

where $\sigma_{M_s}^P$ is the martensitic start transformation stress of porous SMA, σ_0^P is an applied stress, ε_T^P is the strain corresponding to σ_0^P. Since there is no transformation strain in pores, the transformation

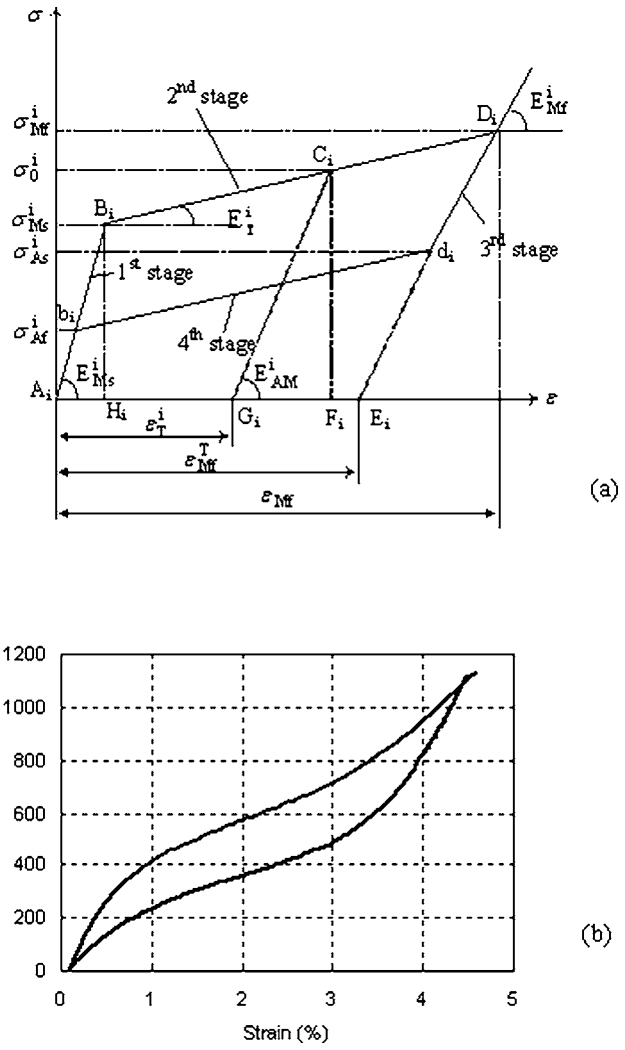

Fig. 3 (*a*) Stress-strain curve of porous or solid sample (*i=P* or *S*), (*b*) stress-strain curve of solid NiTi

strain for porous SMA ε_T^P is the uniform transformation strain in the matrix, i.e., solid NiTi,

$$\varepsilon_T^P = \varepsilon_T^S \equiv \varepsilon_T \tag{24}$$

The above macroscopic strain energy density is set equal to the microscopic stain energy density W_{mi} defined by Eq. (10), where the solution for ε_{ij}^* is obtained from Eqs. (1)–(7) as

$$\varepsilon_{kl}^* = \varepsilon_{kl}^T - \frac{1}{1-f_P}(\mathbf{S}_{klmn} - \mathbf{I}_{klmn})^{-1}\mathbf{C}_{mnij}^{m-1}\sigma_{ij}^0 \tag{25}$$

In Eq. (25), the first term on the right represents the transformation in the solid NiTi matrix; the second term comes from the interactions between pores and applied stress.

Substituting Eq. (25) into Eq. (10), the microscopic strain energy density, W_{mi} is given by

$$W_{mi} = \frac{1}{2}\sigma_{ij}^0\varepsilon_{ij}^0 + \frac{1}{2}f_P\sigma_{ij}^0\left[2\varepsilon_{ij}^T - \frac{1}{1-f_P}(\mathbf{S}_{ijkl} - \mathbf{I}_{ijkl})^{-1}\varepsilon_{kl}^0\right] \tag{26}$$

Since the porous NiTi is subjected to uniaxile load, i.e., $\sigma_{ij}^0 = \{0\ 0\ \sigma_0^P\ 0\ 0\ 0\}^T$, and transformation strain given by $\varepsilon_{ij}^T = \{\nu\varepsilon_T\ \nu\varepsilon_T\ -\varepsilon_T\ 0\ 0\ 0\}^T$, and the pores are assumed to be spherical; thus, Eq. (26) can be reduced to

$$W_{mi} = \frac{1}{2}\sigma_0^P\varepsilon_0 + \frac{1}{2}f_P\sigma_0^P\left[2\varepsilon_T - \frac{1}{1-f_P}\mathbf{Z}_{3333}\varepsilon_0\right] \tag{27}$$

where $\mathbf{Z}_{3333}$ is a component of a 6×6 matrix, $\mathbf{Z}=(\mathbf{S}_{ijkl}-\mathbf{I}_{ijkl})^{-1}$. $\mathbf{S}$ is Eshelby tensor for spherical and ellipsoidal inclusions, respectively. ε_0 is the macroscopic strain of the porous SMA, and it is related to applied stress σ_0^P as

$$\varepsilon_0 = \frac{\sigma_0^P}{E_{AM}} \tag{28}$$

Substituting Eq. (28) into Eq. (27), the microscopic strain energy density W_{mi} of porous NiTi is finally reduced to

$$W_{mi} = \frac{1}{2}\frac{(\sigma_0^P)^2}{E_{AM}} + \frac{1}{2}f_P\sigma_0^P\left(2\varepsilon_T^P - \mathbf{Z}_{3333}\frac{\sigma_0^P}{E_{AM}}\right) \tag{29}$$

where E_{AM} is the Young's modulus of solid (matrix) SMA with ε_T.

By equating the macroscopic strain energy density W_{ma} of Eq. (23) W_{mi} of Eq. (29), and using Eq. (22) with $i=P$, we obtained the following algebraic equation of second-order ε_T as:

$$F(\varepsilon_T)^2 + G\varepsilon_T + H = 0 \tag{30}$$

$$F = \frac{(\gamma\sigma_0^P + \sigma_{M_s}^P)(1-\beta)}{\varepsilon_{M_s}}, \quad G = \gamma\sigma_0^P + \sigma_{M_s}^P + \frac{\sigma_{M_s}^P(1-\beta)(\sigma_{M_s}^P + \sigma_0^P)}{E_{M_s}\varepsilon_{M_f}},$$

$$H = \frac{(1-\alpha)(\sigma_0^P)^2 - (\sigma_{M_s}^P)^2}{E_{M_s}}, \quad \alpha = 1 - \frac{f_P}{1-f_P}\mathbf{Z}_{3333},$$

$$\beta = \frac{E_{M_f}}{E_{M_s}}, \quad \gamma = 1 - 2f_P \tag{31}$$

The solution of ε_T^P, which corresponds to the second kink point D_P in Fig. 3(*a*), is given by

$$\varepsilon_T = \frac{-G + \sqrt{G^2 - 4FH}}{2F} \tag{32}$$

The tangent modulus of the porous SMA is the slope of the second stage of the stress-strain curve shown in Fig. 1, thus, E_T can be expressed in terms of transformation strain ε_T and the stresses, σ_0^P and $\sigma_{M_s}^P$ as

$$E_T = \frac{\sigma_0^P - \sigma_{M_s}^P}{\varepsilon_T} \tag{33}$$

2.2 Unloading Curve. During unloading, the porous SMA material undergoes reverse transformation (martensite phase to austenite phase). Before the applied stress reaches to a critical value σ_{As}^P, the matrix SMA remains 100% martensite phase (first stage of the unloading stress-strain curve in the modeling curve). When the applied stress is decreased to σ_{As}^P, reverse transformation starts and it finishes when the stress reaches another critical value σ_{Af}^P; thereafter, the porous SMA material remains 100% austenite. Therefore, the slope of the first and third stages of the unloading curve is the Young's modulus of the 100% martensite and 100% austenite phase, respectively. The slope of the fourth stage is the same as that of the loading curve in the second stage. Therefore, the Young's moduli of the unloading curve are related to those of the loading curve as

$$E_{As} = E_{M_f} \tag{34a}$$

$$E_T^u = E_T \tag{34b}$$

$$E_{Af} = E_{Ms} \tag{34c}$$

where E_T^u is the slope of the second stage of the unloading curve. The superscript u denotes unloading, whereas those without superscript are the slopes of loading curve.

The austenite start and finish transformation stresses of porous SMA, σ_{As}^P and σ_{Af}^P are related to the corresponding stresses of the solid NiTi by

$$\sigma_{As}^P = (1-f_P)\sigma_{As}^S \tag{35a}$$

$$\sigma_{Af}^P = (1-f_P)\sigma_{Af}^S \tag{35b}$$

where σ_{As}^S and σ_{Af}^S are austenite start and finish transformation stresses of the solid NiTi, respectively. First, we assume that the solid NiTi matrix is isotropic with Poisson's ratio $\nu^A = \nu^M = 0.33$.

3 Model 2: Stress-Strain Curve of Porous NiTi With Open Pores

Here we shall discuss the Eshelby model for a porous SMA with open pores where pores are interconnected (Fig. 4), where unknown fictitious eigenstrain is in pore 1 (ε_{ij}^{*1}) and in pore 2 (ε_{ij}^{*2}) will be determined by Eshelby method. Initially, we distinguish the elastic constant ($\mathbf{C}_{ijkl}$) and eigenstrain (ε^*) associated with pores 1 and those with pores 2, but later we will set those identical to each other as two adjacent pores of the same shape, and orientation should have the same $\mathbf{C}_{ijkl}$ and ε_{ij}^*. There are two steps to obtain the eigenstrains. The first step is to find the eigenstrain ε_{ij}^{*1} and the disturbed stress σ_{ij}^1 in Ω_1 for an infinite body containing ellipsoidal or spherical pores and subjected to uniaxial applied stress σ_0. In the first problem, the other pore Ω_2 is not considered for obtaining ε_{ij}^{*1}, but the interaction between the pores is taken into account by Mori-Tanaka mean field theory. The second step is to find the eigenstrain ε_{ij}^{*2} and disturbed stress σ_{ij}^2 in Ω_2, where the interactions between Ω_1 and Ω_2 is taken into account. After obtaining ε_{ij}^{*1} and ε_{ij}^{*2}, we take the average of these eigenstrains to represent the eigenstrain for the two interconnected pores. The transformation strain ε_T is zero in the first and third stages, since there is no transformation occurring in these two stages, whereas it is not zero in the second and fourth stage. That is the same as in Sec. 2.

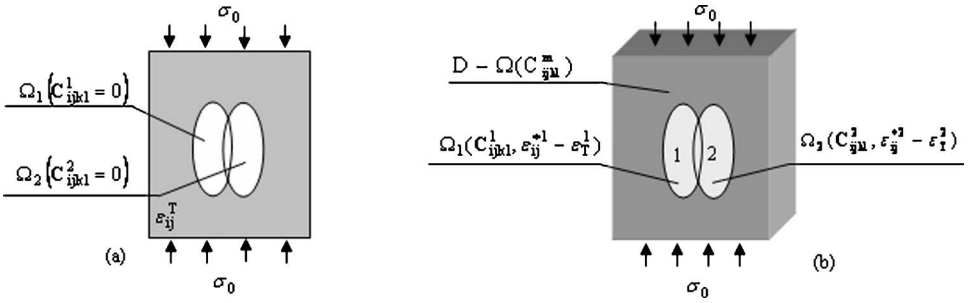

Fig. 4 (*a*) Eshelby's model for interconnected pores in NiTi matrix, which is converted to equivalent inclusion problem (*b*)

3.1 Computation of Average Eigenstrain in Open Pores. In this model, we will simulate the stress-strain curve of a porous SMA with open porosity where two kinds of pore shapes—spherical and ellipsoidal—are used.

3.1.1 Solution of Eigenstrain in Ω_1 Without Ω_2, ε^{**1}_{ij}. The Eshelby model for finding ε^{**1}_{ij} is the same as the in model 1; therefore, we list only the final solutions

$$\varepsilon^{**1}_{kl} = -\frac{1}{1-f_P}(\mathbf{S}_{klmn} - \mathbf{I}_{klmn})^{-1}\mathbf{C}^{m-1}_{mnij}\sigma^0_{ij} \tag{36}$$

3.1.2 Solution of Eigenstrain in Ω_2 by Accounting Interactions Between Ω_1 and Ω_2, ε^{**2}_{ij}. In this step, the disturbed stress in Ω_2 is obtained in terms of ε^{**2}_{ij}, which is unknown thus far. In the first problem, disturbed stress outside the end of the Ω_1, σ^{-1}_{ij} is expressed in terms of σ^1_{ij}. Then the total stress σ^t_{ij} in Ω_2 vanishes

$$\sigma^t_{ij} = \sigma^0_{ij} + \sigma^2_{ij}(\varepsilon^{**2}_{ij}) + \sigma^{-1}_{ij} = 0 \tag{37}$$

where $\sigma^2_{ij}(\varepsilon^{**2}_{ij})$ is the self-stress in Ω_2 induced by eigenstrain ε^{**2}_{ij} The disturbed stress σ^{-1}_{ij} is given by the formula of Hill-Walpole-Mura jump condition [17]

$$\sigma^{-1}_{ij} - \sigma^1_{ij} = \mathbf{C}_{ijkl}(-\mathbf{C}_{pqmn}\varepsilon^{**1}_{mn}M_{kp}n_q n_l + \varepsilon^{**1}_{kl}) \tag{38a}$$

where

$$M_{kp} = \frac{\left\lfloor \frac{\delta_{kp} - n_k n_p}{2(1-\nu)} \right\rfloor}{\mu} \tag{38b}$$

and where n_i is the ith component of an unit vector outer normal to the inclusion and is given by

$$n = (1\ 0\ 0) \tag{38c}$$

It is noted in Fig. 4 that the interconnection between Ω_1 and Ω_2 is at the equator region with its normal base vector pointing to x_1-axis. With Eq. (38*c*), Eq. (38*a*) yields

$$\sigma^{-1}_{ij} = \sigma^1_{ij} + \mathbf{C}_{ij11}(-\mathbf{C}_{11mn}\varepsilon^{**1}_{mn}M_{11} + \varepsilon^{**1}_{11}) \tag{39}$$

$$\text{where } M_{11} = \frac{(1+\nu)(1-2\nu)}{E(1-\nu)} \tag{40}$$

The applied stress is given as

$$\sigma^0_{ij} = (0\ 0\ \sigma^0\ 0\ 0\ 0) \tag{41}$$

Stress in Ω_2 in terms of eigensrain ε^{**2}_{ij} is given by

$$\sigma^2_{ij} = (1-f_P)\mathbf{C}^m_{ijkl}(\mathbf{S}_{klmn} - \mathbf{I}_{klmn})\varepsilon^{**2}_{mn} \tag{42}$$

By substituting Eq. (39), (41), and (42) into Eq. (37), we obtain eigenstrain in Ω_2 ε^{**2}_{ij} as

$$\varepsilon^{**2}_{mn} = \mathbf{\Pi}_{mnrs}\varepsilon^{**1}_{rs} \tag{43a}$$

$$\text{where } \mathbf{\Pi}_{mnrs} = -(\mathbf{S}_{mnpq} - \mathbf{I}_{mnpq})^{-1}(-\mathbf{C}_{pqrs}M_{11} + \mathbf{I}_{pqrs})/(1-f_P) \tag{43b}$$

We take average of the eigenstrains in Ω_1 and Ω_2 to represent the eigenstrain of all interconnected pores

$$\varepsilon^{**}_{mn} = \frac{1}{2}(\varepsilon^{**1}_{mn} + \varepsilon^{**2}_{mn}) = \frac{1}{2}(\mathbf{\Pi}_{mnrs} + \mathbf{I}_{mnrs})\varepsilon^{**1}_{rs} \tag{44}$$

Once the average eigenstrain ε^{**}_{mn} is obtained, we can use the first model to calculate the moduli and critical stresses. Therefore, we list only the final useful for the moduli and critical stresses in the following.

3.2 Elastic Moduli at Stage I and III. Since there is no transformation at stage I and III, the Young's modulus of each stage can be obtained by equivalency of energy density as in model 1 from Eq. (11). Therefore, the Young's modulus of stage I is given as

$$\frac{E_{M_s}}{E_A} = \frac{1}{1 + \mathbf{D}_{3333}f_P} \tag{45a}$$

and that of stage III is

$$\frac{E_{M_f}}{E_M} = \frac{1}{1 + \mathbf{D}_{3333}f_P} \tag{45b}$$

where $\mathbf{D}_{3333}$ is a component of a 6×6 matrix $\mathbf{D}_{klrs}$, which is given as

$$\mathbf{D}_{klrs} = -\frac{\mathbf{A}_{klmn}\cdot\mathbf{B}_{mnpq}\cdot\mathbf{C}_{pqrs}}{2(1-f_P)} \tag{46}$$

where $\mathbf{A}_{klmn} = \mathbf{I}_{klmn} + \mathbf{\Pi}_{klmn}$, $\mathbf{B}_{mnpq} = (\mathbf{S}_{mnpq} - \mathbf{I}_{mnpq})^{-1}$, $\mathbf{C}_{pqrs} = \mathbf{C}^{-1}_{pqrs}$.

3.3 Tangent Stiffness of Stage II and IV. To obtain E_T, first we have to obtain the transformation strain ε_T. The transformation strain is obtained in the same manner as that in model 1

$$\varepsilon_T = \frac{(-G_2 + \sqrt{G_2^2 - 4G_1G_3})}{2G_1} \tag{47}$$

where

$$G_1 = [\sigma^p_{M_s} + (1-f_P)\sigma^p_0]\xi_1 \tag{48a}$$

$$G_2 = f_P\sigma^p_0E_A - f_PD_{3333}(\sigma^p_0)^2\xi_1 - (\sigma^p_{M_s} + \sigma^p_0)E_A - \xi_1\xi_2 \tag{48b}$$

Table 1 Input data given by solid NiTi reference curve

σ^s_{Ms}	σ^s_{Mf}	σ^s_{Af}	E_A	E_M	ε_{Ms}	ε_{Mf}
420 MPa	780 MPa	450 MPa	75 GPa	31 GPa	0.0053	0.04

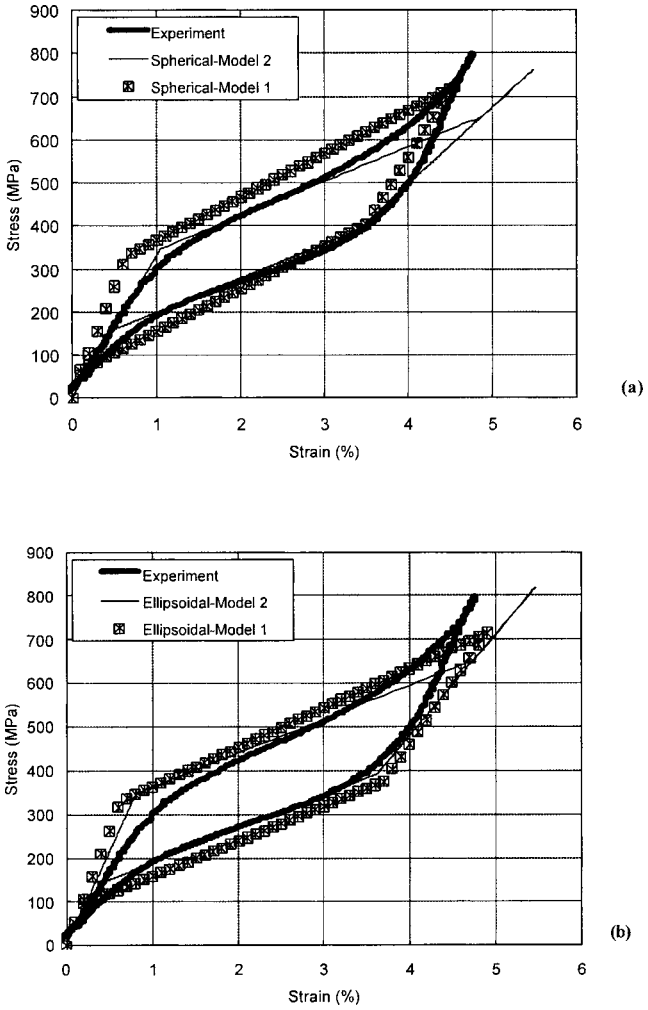

Fig. 5 Comparison of the experimental data to predictions by the present two models

$$G_3 = \xi_2 E_A - \sigma^p_{M_s}\sigma^p_0 + f_p D_{3333}(\sigma^p_0)^2 E_A \tag{48c}$$

and

$$\xi_1 = \frac{(E_A - E_M)}{(\varepsilon_{M_f} - \sigma^p_{M_s}/E_M)} \tag{49a}$$

$$\xi_2 = \frac{(\sigma^p_{M_s} + \sigma^p_0)\sigma^p_{M_s}}{E_{M_s}} \tag{49b}$$

Therefore, the tangent modulus, E_T is given in terms of transformation strain as

$$E_T = \frac{\sigma^P_0 - \sigma^P_{M_s}}{\varepsilon_T} \tag{50}$$

Table 2 Comparison of the critical stresses and Young's moduli of experimental data and predictions by two models

	E_{Ms} (GPa)	E_T (GPa)	E_{Mf} (GPa)
Experimental	41.0	8.0	27.0
Ellipsoidal pore—Model 1	52.6	9.2	23.7
Spherical pores—Model 1	52.6	10.1	22.7
Ellipsoidal pore—Model 2	43.2	7.7	23.2
Spherical pores—Model 2	33.2	7.9	17.9

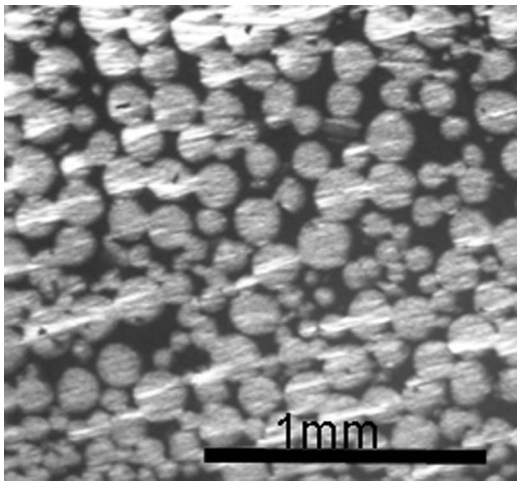

Fig. 6 Microstructure of 13% porosity specimen

3.4 Critical Stress. The four critical stresses are obtained in the same manner as that in model 1. They are given by

$$\sigma^P_{M_s} = (1 - f_P)\sigma^S_{M_s} \tag{51a}$$

$$\sigma^P_{M_f} = (1 - f_P)\sigma^S_{M_f} \tag{51b}$$

$$\sigma^P_{As} = (1 - f_P)\sigma^S_{As} \tag{51c}$$

$$\sigma^P_{Af} = (1 - f_P)\sigma^S_{Af} \tag{51d}$$

It is noted here that superscripts S and P denote solid and porous SMA, respectively.

4 Discussion

We use Ti-50.9 at. %Ni as SMA, and the experimental data of the stress-strain curve of solid NiTi under compressive loading is made into piecewise linear wire four stages, Fig. 3(*a*). Table 1 shows the input data of the piecewise linearized stress-strain curve of solid NiTi to simulate the stress-strain curve of 13% porosity NiTi specimen [11].

Figure 5 shows the stress-strain curves predicted by models 1 and 2. Table 2 lists the values of the critical stresses and Young's

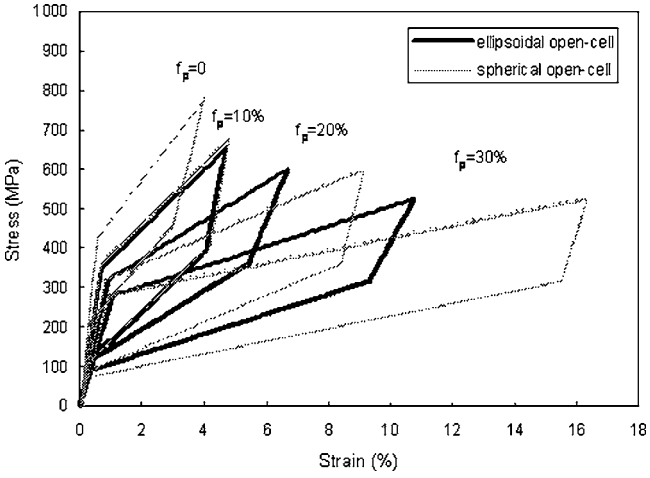

Fig. 7 Stress-strain curves predicted by ellipsoidal and spherical open-cell model

moduli predicted by two models, as well as the experiment [11]. The comparison shows that the simulations have reasonable good agreement with the experimental data.

It is noted that the stress-strain curve of the ellipsoidal pore-shape assumption is closer to the experimental curve than that of the spherical pore-shape assumption. This indicates that the ellipsoidal pore shape is more likely the realistic pore shape in the specimen used for the experiment. Figure 6 shows the microstructure of the porous NiTi specimen. Although, from this figure we can see that the realistic pore shape is not ellipsoidal, but the ellipsoidal is closer than the spherical to the realistic shape. Therefore, the model with ellipsoidal pore shape predicts more accurately.

Comparing the stress-strain curves predicted by Models 1 and 2, we can see that model 2 is more accurate than model 1. This is because model 2 takes into account the interactions between two adjacent pores by assuming they are interconnecting to each other. Figure 6 supports this assumption that pores are indeed interconnected. Model 2 can take account for the interaction between the interconnected pores; therefore, the predictions by model 2 give rise to closer agreement with the experiment.

Figure 7 shows how the porosity f_P influents stress-strain curve predicted by model 2, the open-cell model. It is found in Fig. 7 that when the porosity is $<10\%$, the ellipsoidal and spherical shapes have almost same prediction; but once when the porosity gets larger and larger, the difference between the two shapes increases dramatically.

5 Conclusion

Two models predicting the stress-strain curve of porous SMA subjected to compressive load are presented. Pores are treated as separate individuals in model 1, whereas they are interconnected to each other in model 2. Both models explain the experimental data reasonably well. Model 2, which can take account for the interactions among interconnected pores, provides better predictions than model 1 in predicting the experimental data of the Young's moduli of porous NiTi.

Acknowledgment

The present work was supported by a grant from ONR-MURI project (N-000140210666) via University of California at San Diego, where PI is Professor S. Nemat-Nasser. The program monitor at ONR is Dr. R. Barsoum.

References

[1] Lagoudas, D. C., Strelec, J. K., Yen, J., and Khan, M. A., 2001, "Intelligent Design Optimization of a Shape-Memory-Alloy-Actuated Reconfigurable Wing," Proc. SPIE, **3984**, pp. 338–348.
[2] Garner, L. N., Wilson, L. J., Lagoudas, D. C., and Rediniotis, O. K., 2000, "Development of a Shape Memory Alloy Actuated Biomimetic Vehicle," Smart Mater. Struct., **9**, pp. 673–683.
[3] Martynova, I., Skorohod, V., and Solonin, S., 1991, "Shape Memory and Superelasticity Behavior of Porous Ti-Ni Material," J. Phys. IV, **1991**, pp. C4/421–C4/426.
[4] Goncharuk, N. V., Martynova, I., Naidenova, I. F., and Skorokhod, O. R., 1992, "Superelaticity and Shape Memory of Sintered Porous Titanium Nickelide," Poroshk. Metall. (Kiev), **4**, pp. 56–60.
[5] Li, Y. H., Rong, L. J., and Li, Y. Y., 1998, "Porous NiTi Alloy Prepared From Elemental Powder Sintering," J. Mater. Res., **13**, pp. 2847–2851.
[6] Li, Y. H., Rong, L. J., Luo, X. H., and Li, Y. Y., 2000, "Microstructure and Superelaticity of Porous NiTi Alloy," Sci. China, Ser. E: Technol. Sci., **E-42**, pp. 94–101.
[7] Li, B. Y., Rong, L. J., and Li, Y. Y., 1998, "Transformation Behavior of Sintered Porous NiTi Alloys," Metall. Mater. Trans. A, **30A**, pp. 2753–2756.
[8] Yuan, B., Chung, C. Y., and Zhu, M., 2004, "Microstructure and Martensitic Transformation Behavior of Porous NiTi Shape Memory Alloy Prepared by Hot Isostaic Pressing Processing," Mater. Sci. Eng., A, **382**, pp. 181–187.
[9] Li, B. Y., Rong, L. J., Gjuanter, V. E., and Li, Y. Y., 2000, "Porous NiTI Shape Memory Alloys Produced by Two Different Methods," Z. Metallkd., **91**, pp. 291–295.
[10] Lagoudas, D. C., Entchev, P. B., and Vandygriff, E. C., 2000, "Modeling of Thermomehcanical Response of Porous Shape Memory Alloys," Proc. SPIE, **3992**, pp. 141–153.
[11] Zhao, Y., Taya, M., Kang, Y. S., and Kawasaki, A., 2005, "Compressive Behavior of Porous NiTi Shape Memory Alloy," Acta Mater., **53**(2), pp. 337–343.
[12] Eshelby, J. D., 1957, "The Determination of the Elastic Field of an Ellipsoidal Inclusion, and Related Problems," Proc. R. Soc. London, Ser. A, **3**, pp. 376–396.
[13] Tanaka, K., and Mori, T., 1973, "Average Stress in Matrix and Average Elastic Energy of Materials With Misfitting Inclusions," Acta Metall., **21**, pp. 571–574.
[14] Mura, T., 1987, *Micromechanics of Defects in Solids*, 2nd ed., Martinus Nijhoff, Dordrecht, pp. 168–170.
[15] Taya, M., and Chou, T. W., 1981, "On Two Kinds of Ellipsoidal Inhomogeneities in an Infinite Elastic Body: An Application to a Hybrid Composite," Int. J. Solids Struct., **136**, pp. 553–563.
[16] Taya, M., and Mura, T., 1981, "On Stiffness and Strength of an Aligned Short-Fiber Reinforced Composite Containing Fiber-End Cracks Under Uniaxial Applied Stress," ASME J. Appl. Mech., **48**, pp. 361–367.
[17] Arsenault, R. J., and Taya, M., 1987, "Thermal Residual Stress in Metal Matrix Composite," Acta Metall., **35**, pp. 651–659.